Journal of Statistical Physics, Vol. 128, Nos. 1/2, July 2007 (© 2007)
DOI: 10.1007/s10955-006-9204-x

A Theoretical Approach to Actin Filament Dynamics

Jifeng Hu,[1] Anastasios Matzavinos[1] and Hans G. Othmer[1,2]

Received February 15, 2006; accepted August 28, 2006
Published Online: September 26, 2006

Dynamic control of the actin network in eukaryotic cells plays an essential role in their movement, but to date our understanding of how the network properties are controlled in space and time is still rudimentary. For example, how the cell maintains the pools of monomeric actin needed for a rapid response to signals, how the filament length distribution is controlled, and how the actin network properties are modulated by various bundling and severing proteins to produce the mechanical response is not known. Here we address the simplest aspect of this, which is to understand the temporal evolution of the length distribution *in vitro* in order to understand what the relevant time scales are for establishment of a time-invariant distribution. Surprisingly, we find that there are very long-lived intermediate length distributions that are not exponential. The results shed light on the time scale needed to observe genuine steady-state distributions, and emphasize the necessity of control molecules for modulating the time scale.

KEY WORDS: cell motility, actin filaments, mathematical modeling

1. INTRODUCTION

Cell movement is an essential process at various stages in the life cycle of most organisms. Early development of multicellular organisms involves individual and collective cell movement, leukocytes must migrate toward sites of infection as part of the immune response, and in cancer directed movement is involved in invasion and metastasis. Movement entails force generation within cells and force transmission to their surroundings via adhesion sites, and understanding how they are controlled in space and time to produce cell-level movement is a major challenge.

[1] School of Mathematics, University of Minnesota, Minneapolis, MN 55455, USA. Research supported in part by NSF grants DMS 9805494 and DMS 0317372.
[2] Also in the Digital Technology Center, University of Minnesota. Research supported in part by NIH grant GM 29123, the Max Planck Institute for Mathematics in the Sciences and the Alexander von Humboldt Foundation; e-mail: othmer@math.umn.edu.

The mechanical interactions are mediated by the cytoskeleton, which is a network of actin filaments, intermediate filaments, and microtubules in the cytoplasm, and spatially- and temporally-controlled deformation and remodeling of the cytoskeleton are essential for movement. Its stress/strain response can be varied from that of a solid to that of a liquid by controlled assembly, cross-linking, and disassembly of its components. The biochemical control processes, the microstructure of the cytoskeleton, and the formation and dissolution of adhesion sites are coordinated at the whole-cell level to produce the forces needed for movement.

1.1. Actin Filaments: Polymerization, Treadmilling, and Length Distribution

Actin filaments (F-actin) are morphologically asymmetric, with a barbed or plus end at which monomer addition is faster than at the minus or pointed end. *In vitro* the filaments are flexible and buckle easily, but *in vivo* cells create a dense network of short, branched filaments by tightly coupling nucleation, branching, and cross-linking of filaments in the lamellipodium, a thin (0.1–0.2 μm), sheet-like protrusion filled with actin.[3,25] The stiffness of the network enables new filaments to exert force on the membrane and provides the structural basis for polymerization-driven protrusion.

Proteins that control actin filament turnover are spatially-regulated so as to produce actin assembly at the front and disassembly at the rear of the lamellipodium, a process called treadmilling.[27] These control proteins can be grouped by their function as follows.

- Sequestering proteins: these sequester actin monomers to prevent spontaneous nucleation of filaments ($\beta-$thymosins) or interact with actin monomers to enhance nucleotide exchange (profilin).
- Crosslinking proteins: these cross-link the actin filaments and can induce a sol-to-gel transition. An example is α-actinin. Others such as vinculin, talin, and zyxin link the cortex (the network adjacent to the membrane) to the plasma membrane.
- Severing proteins: these sever F-actin to generate more filament ends for assembly or disassembly. These include the ADF (actin depolymerization factor/cofilin) family of proteins and gelsolin.
- Other proteins function to cap filament ends to regulate addition or loss of actin subunits (capping protein, gelsolin, the Arp2/3 complex), to nucleate filament growth (the Arp2/3 complex, formin), or to enhance subunit dissociation by cofilin.

Despite the high concentrations of the globular monomeric form of actin (G-actin) in many cells, filaments rarely nucleate spontaneously *in vivo* in the

presence of profilin and thymosin-4.[22] These sequestering proteins maintain a pool of actin, which, in the case of profilin, is available for polymerization as soon as new barbed ends are created.[22] However, cells such as *Dictyostelium discoideum* lack both, so the picture is undoubtedly more complex (see also. Ref. 28.)

The Arp2/3 complex, so called because it contains the actin-related proteins, Arp2 and Arp3, nucleates new actin filament assembly, probably in response to signals such as the activation of receptor tyrosine kinases or receptors coupled to small GTPases of the Rho family (e.g., Rho, Rac, and Cdc42–[12,26]). *In vitro*, the Arp2/3 complex induces branching of actin filaments, caps the slow-growing (pointed) end of filaments, and nucleates actin assembly.[17] Its activity can be greatly stimulated by direct interaction with proteins of the WASP family.[12,26]

The mechanism by which ADF/cofilin proteins control the filament size distribution is not completely clear. Initially severing was thought to be a major factor, but Carlier *et al.*[1] showed that recombinant ADF/cofilin proteins enhanced the on-rate at the barbed end up to 12-fold and the off-rate at the pointed ends up to 22-fold, thereby increasing treadmilling 25-fold, without severing filaments. More recently Moriyama *et al.*[16] found that porcine cofilin increased filament numbers by severing filaments with a maximum of approximately one severing event per 290 actin subunits ($\sim$0.8 μm in length). Off-rates of G-ADP, which is the rate-limiting step were also enhanced to a maximum of $\sim$6.4-fold. Mutant forms of cofilin were identified that differentially affected severing or the enhanced off-rate at the pointed end. Results in yeast suggest that ADF/cofilin-stimulated filament severing plays an essential role, independent of any effect on depolymerization. A summary of how the sequestering and severing proteins contribute to maintaining the filament length is shown in Fig. 1.

Thus there is control of monomeric actin pools via sequestration in a number of states, control of filament growth by capping of filament ends with gelsolin and other capping proteins, and breakage of filaments via ADF/cofilin, and annealing of filaments. The interplay between these factors and others produces a dynamically-varying distribution of actin filament lengths. One example is shown in Fig. 2, which is for a relatively simple situation, wherein either there is only actin monomer initially (A) (albeit there is a protein phallodine that stabilizes long filaments), or actin plus a severing protein (severin) (B). The dramatic shift of these 'steady-state' length distributions is one of many observations that remain to be explained by mathematical modeling and analysis.

1.2. Theoretical Approaches to the Dynamics of Actin Filament Length Distribution

Actin filament dynamics have been studied both analytically and computationally in the last three decades and the studies fall into two broad categories. The

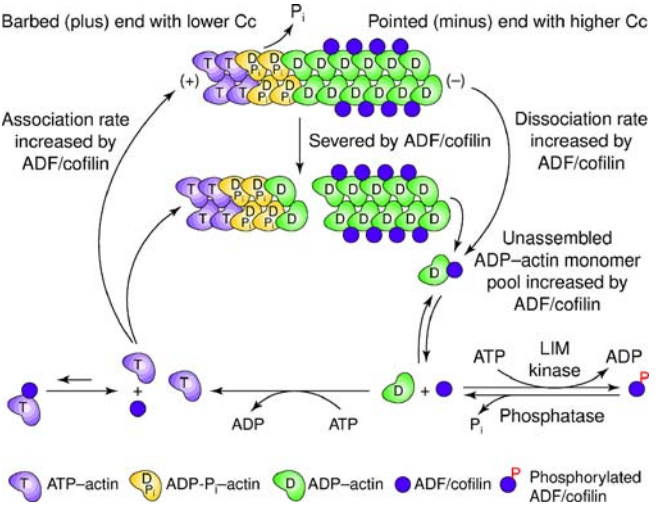

Fig. 1. A schematic of the effects of ADF/cofilin and profilin on filament length (From[2]). **[color online]**.

first is characterized by a focus on individual actin filaments – or actin filament networks – as a component of a more complex system. The questions addressed include the postulated mechanisms for polymerization-driven force generation by individual filaments abutting a surface, such as a cell's membrane or the surface of a polystyrene bead,[4,14,15,21] and the mechanism for symmetry breaking in actin filament networks and force generation by such networks.[7,20] A recent review of this approach is given in Ref. 13.

The second approach focuses on spontaneous polymerization of highly purified actin monomers. Experimental conditions can be controlled more precisely than *in vivo*, and this leads to simpler mathematical models that can be analyzed in

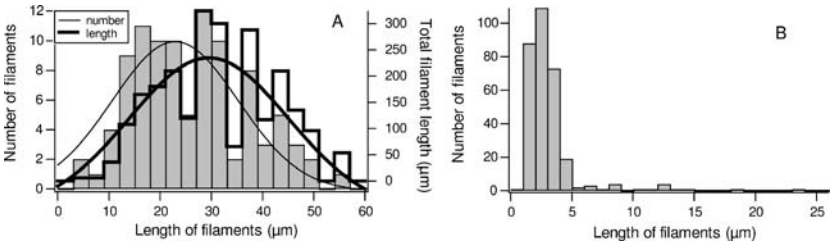

Fig. 2. A. The size distribution of actin filaments in a 10 μM solution of purified G-actin, as determined by fluorescence of phalloidine-rhodamine tagged actin. B. In the presence of severin at a severin:actin ratio of 1:1000 they find a Poisson distribution of mean length $L \sim 3\ \mu$m (From Ref. 11).

detail. The main interest here is the steady-state length distribution and the statistical properties of the dynamics of an ensemble of actin filaments. As we will see later, the steady state analysis is easily done, but the dynamics of the approach to a steady state is more difficult. Indeed, despite the influential theoretical treatment of actin polymerization by Oosawa and Asakura [18] there are still significant open questions concerning the dynamics of the simplest system (*cf.*, *e. g.* Ref. 10)

Our focus here is on the second aspect of actin filament dynamics, in particular, on characterizing the dynamic length distribution of filaments in a solution of highly purified monomers. This work is a first step toward understanding more complex phenomena such as the dynamics of the associated nucleotide compositions of actin filaments under a variety of polymerization conditions and the effects of various control molecules on the dynamics. We begin by reviewing some previous experimental and theoretical work on this problem; other references to related work will be made later in the appropriate context.

Sept *et al.* [24] measured the lengths of actin filaments formed by spontaneous polymerization of purified actin monomers and found that the steady-state length distributions are exponential with a mean of about 7 μm independent of the initial actin monomer concentration. As will be seen (and is well known), this independence of the initial concentration is inconsistent with the original nucleation-elongation mechanism proposed by Oosawa and Asakura. [18] Thus Sept *et al.* [24] formulated a deterministic model that incorporates nucleation but lumps all filaments of length greater than four monomers into one pool, and investigated the mechanisms underlying their experimental result. They showed that this successfully fits experimental data for the time course of polymerization *and* for the mean length of the distribution, and they suggest that although the simple elongation-nucleation mechanism is able to describe the time course of polymerization, it seriously underestimates the average length. They conclude that the additional steps of filament fragmentation and annealing represent a minimal extension to the basic nucleation-elongation theory necessary to explain both the observed time course of polymerization and the mean length.

It was found in Ref. 24 that the model fails to fit experimental data at low actin concentrations, which is expected since assumptions such as the existence of a reptation tube associated with each actin filament are no longer valid in this regime. In addition, the fact that all filaments of length greater than four are lumped in the model precludes predictions about the length distribution and requires neglect of the depolymerization of the shortest filaments. Information about higher moments of the length distribution cannot be extracted from this approach and the important aspect of length fluctuations cannot be addressed. One of our objectives is to understand the evolution of the length distribution, and in particular, the characteristic time scale for the establishment of a steady state distribution. We find that, beginning with a pure monomer pool, the distribution quickly evolves to a 'quasi-attractor' for which the length distribution has a maximum at an

intermediate length, and we provide an explanation for the experimentally-observed 'polymerization' and 'diffusion' stages in the evolution. In future work we will analyze the effects of fragmentation and annealing on the dynamics.

2. THE POLYMERIZATION MODEL

Let $\mathcal{M}_n$ denote a filament of length n,[3] and let C_n be the corresponding concentration. The kinetic scheme that describes the polymerization steps considered is as follows.

$$\underbrace{\mathcal{M}_1 + \mathcal{M}_1 \underset{k_1^-}{\overset{k_1^+}{\rightleftarrows}} \mathcal{M}_2 \underset{k_2^-}{\overset{k_2^+ \mathcal{M}_1}{\rightleftarrows}} \mathcal{M}_3}_{\text{Nucleation}} \quad \underbrace{\underset{k_3^-}{\overset{k_3^+ \mathcal{M}_1}{\rightleftarrows}} \mathcal{M}_4 \quad \cdots \mathcal{M}_n \underset{k_n^-}{\overset{k_n^+ \mathcal{M}_1}{\rightleftarrows}} \mathcal{M}_{n+1} \cdots}_{\text{Propagation}}$$

In the numerical computations described later we use kinetic constants reported by Sept *et al.*,[24] which are $k_1^- = 10^6\,\mathrm{s}^{-1}$, $k_2^- = 10^3\,\mathrm{s}^{-1}$, and $k_n^- = 1\,\mathrm{s}^{-1}$ for all $n \geq 3$ and $k_n^+ = 10\,\mu\mathrm{M}^{-1}\,\mathrm{s}^{-1}$, for all $n \leq N$. The first two steps, which lead to formation of dimers and trimers, are distinguished in the above diagram by virtue of the fact that dissociation rates are extremely rapid for these steps, and thus it is difficult in a pure monomer solution to initiate filaments. Assuming mass-action kinetics for the monomer addition and release, the above kinetic scheme leads to the system of ordinary differential equations

$$\begin{aligned}
\frac{dC_1}{dt} &= -2\left(k_1^+ C_1^2 - k_1^- C_2\right) - \sum_{n=3}^{N} \left(k_{n-1}^+ C_1 C_{n-1} - k_{n-1}^- C_n\right) = -2J_2 - \sum_{n=3}^{N} J_n \\
&\vdots \\
\frac{dC_n}{dt} &= \left(k_{n-1}^+ C_1 C_{n-1} - k_{n-1}^- C_n\right) - \left(k_n^+ C_1 C_n - k_n^- C_{n+1}\right) = J_n - J_{n+1} \\
&\vdots \\
\frac{dC_N}{dt} &= \left(k_{N-1}^+ C_1 C_{N-1} - k_{N-1}^- C_N\right) = J_N
\end{aligned} \tag{1}$$

Here the flux J_n from a filament of length $n-1$ into a filament of length n is defined as

$$J_n \equiv k_{n-1}^+ C_1 C_{n-1} - k_{n-1}^- C_n. \tag{2}$$

In a thermodynamically open system it is reasonable to consider the limit $N \to \infty$, but we only consider a closed system, in which the total amount of monomer is fixed

[3] We refer to the length in units of monomers, but since actin filaments are two-stranded the unit of length is actually the half-length of a monomer.

by the initial composition, and therefore we supplement (1) with the conservation condition

$$\sum_{n=1}^{N} nC_n = C_0, \tag{3}$$

where C_0 is the total initial concentration of actin (either in filaments or in the globular form).

To nondimensionalize (1) and (3), we define $u_n \equiv C_n/C_0$, and $\tau \equiv t/T$, where T will be chosen later to emphasize different aspects of the dynamics. Then (1) may be rewritten as

$$\begin{aligned}
\frac{du_1}{d\tau} &= -2\left(\kappa_1^+ u_1^2 - \kappa_1^- u_2\right) - \sum_{n=3}^{N}\left(\kappa_{n-1}^+ u_1 u_{n-1} - \kappa_{n-1}^- u_n\right) = -2j_2 - \sum_{n=3}^{N} j_n \\
&\vdots \\
\frac{du_n}{d\tau} &= \left(\kappa_{n-1}^+ u_1 u_{n-1} - \kappa_{n-1}^- u_n\right) - \left(\kappa_n^+ u_1 u_n - \kappa_n^- u_{n+1}\right) = \quad j_n - j_{n+1} \\
&\vdots \\
\frac{du_N}{d\tau} &= \left(\kappa_{N-1}^+ u_1 u_{N-1} - \kappa_{N-1}^- u_N\right) = \quad j_N
\end{aligned} \tag{4}$$

where for all $n \leq N$,

$$\kappa_n^+ = k_n^+ C_0 T \quad \text{and} \quad \kappa_n^- = k_n^- T \tag{5}$$

It is clear that the set

$$\Omega \equiv \left\{ u_n \mid 0 \leq u_n \leq 1, \quad \sum_{n=1}^{N} n u_n = 1 \right\}$$

is closed and bounded, and is invariant for all $t \geq 0$, and therefore the solution of (4)–(5) exists for all time.

2.1. Analysis of the Steady State

At steady state the fluxes between filaments vanishes and one finds that the steady state dimensionless concentrations are

$$u_n^s = K_{n-1} u_1^s u_{n-1}^s = K_{n-1} K_{n-2} \left(u_1^s\right)^2 u_{n-2}^s = \cdots = \left(\prod_{i=1}^{n-1} K_i\right) \left(u_1^s\right)^n \tag{6}$$

where $K_n \equiv \kappa_n^+/\kappa_n^-$. The conservation condition for the steady-state distribution becomes

$$f(N, u_1) \equiv \sum_{n=1}^{N} n u_n = \sum_{n=1}^{N} n \Lambda_n \left(u_1^s\right)^n = 1 \tag{7}$$

where $\Lambda_n = \prod_{i=1}^{n-1} K_i$. The left-hand side of (7) is monotone increasing with respect to u_1^s and vanishes at zero, which implies that the steady-state u_1^s is unique. The unique steady-state solution $(u_1^s, u_2^s, \cdots, u_N^s)$ can be found by solving this for u_1^s and then back substituting into (6).

Clearly f is monotone increasing in u_1 for fixed N and monotone increasing in N for fixed $u_1 > 0$. If in addition we assume that $\kappa_n^+ = \kappa^+$ for all $n < N$, $\kappa_n^- = \kappa^-$ for all $n \geq 3$, and define $K = \kappa^+/\kappa^-$, then $u_n^s/u_{n-1}^s = K u_1$ for $n \geq 4$. It follows that if $f(N, K^{-1}) < 1$, $u_1^s > K^{-1}$ and the steady distribution is monotone increasing for $n \geq 4$, while if $f(N, K^{-1}) > 1$ the distribution is monotone decreasing. Thus $u_1 = K^{-1}$ defines a critical concentration that in dimensional form is given by $C_1 = k^-/k^+$. It is also clear that one can always choose N so large that the distribution is monotone decreasing. In light of the scaling by C_0, this puts conditions on the relationship between C_0 and N in order to achieve either a monotone increasing or decreasing profile (for $n \geq 4$). That u_3^s respects the monotonicity of the tail $n \geq 4$ is also clear. It might appear that only monotone decreasing profiles are physically relevant, but this is not the case; in a confined geometry such as a vesicle, the size of the system may impose a relatively small upper bound on N. Other authors have derived the decreasing exponential distribution when $N = \infty$ (cf Ref. 5 and references therein), but not the increasing exponential solutions.

2.2. Convergence to the Steady State

Next we show that the free energy defined below provides a Lyapunov function for the dynamics, and thus all solutions converge to the unique steady state asymptotically in time. Since quantities other than the monomer and filament concentrations enter the definition of the free energy, it proves convenient to revert to the dimensional form of the equations. Consider the general monomer addition step

$$\mathcal{M}_1 + \mathcal{M}_{n-1} \underset{k_{n-1}^-}{\overset{k_{n-1}^+}{\rightleftarrows}} \mathcal{M}_n \qquad n = 2, \ldots, N$$

with rate $J_n = k_{n-1}^+ C_1 C_{n-1} - k_{n-1}^- C_n$ in a closed system. The affinity of this reaction is given by

$$A_n = \mu_1 + \mu_{n-1} - \mu_n$$

where the chemical potentials are defined as

$$\mu_n = \mu_n^0(T, P) + RT \ln \frac{C_n}{C_T} = \mu_n^0(T, P) + RT \ln x_n.$$

Here x_n is the mole fraction of species n and C_T is the total concentration, including water. Since actin solutions are typically in the 10 – 100 μM range,[22] we can ignore the small changes in total concentration that accompany polymerization and thus assume that C_T is constant at constant temperature and pressure. The change in the Gibbs free energy

$$G = \sum_{n=1}^{N} x_n \mu_n$$

is given by

$$\frac{dG}{dt} = -\frac{\Phi}{C_T},$$

where the dissipation function Φ is

$$\begin{aligned}\Phi &= \sum_{n=2}^{N} A_n J_n \\ &= \sum_{n=2}^{N} \left(\Delta\mu_n^0 + RT \ln \frac{C_1 C_{n-1}}{C_T C_n} \right) (k_{n-1}^+ C_1 C_{n-1} - k_{n-1}^- C_n).\end{aligned}$$

The Gibbs-Duhem relation has been used to eliminate one factor in deriving this. At thermodynamic equilibrium $A_n = 0$, and therefore

$$-\Delta\mu_n^0 = RT \ln \frac{C_1^s C_{n-1}^s}{C_T C_n^s}.$$

It follows that

$$\begin{aligned}\Phi &= \sum_{n=2}^{N} \left[RT \ln \left(\frac{C_1 C_{n-1}}{C_T C_n} \cdot \frac{C_T C_n^s}{C_1^s C_{n-1}^s} \right) \right] \left(k_{n-1}^+ C_1 C_{n-1} - k_{n-1}^- C_n \right) \\ &= RT \sum_{n=2}^{N} \left(k_{n-1}^+ C_n C_T \right) \left[\ln \left(\frac{C_1 C_{n-1}}{C_T C_n} \cdot \frac{C_T C_n^s}{C_1^s C_{n-1}^s} \right) \right] \left(\frac{C_1 C_{n-1}}{C_T C_n} - \frac{k_{n-1}^-}{k_{n-1}^+ C_T} \right) \\ &= RT \sum_{n=2}^{N} \left(k_{n-1}^+ C_n C_T \right) \left[\ln \left(\frac{C_1 C_{n-1}}{C_T C_n} \cdot \frac{C_T C_n^s}{C_1^s C_{n-1}^s} \right) \right] \left(\frac{C_1 C_{n-1}}{C_T C_n} - \frac{C_1^s C_{n-1}^s}{C_T C_n^s} \right)\end{aligned}$$

Define

$$\Lambda_n = \frac{C_1 C_{n-1}}{C_T C_n}, \quad \Lambda_n^* = \frac{C_T C_n^s}{C_1^s C_{n-1}^s}$$

Then

$$\Phi = RT \sum_{n=2}^{N} \frac{k_{n-1}^+ C_n C_T}{\Lambda_n^*} \cdot (\Lambda_n \Lambda_n^* - 1) \cdot \ln(\Lambda_n \Lambda_n^*)$$

and this is of the form

$$\Phi = \sum a_n (z_n - 1) \ln z_n$$

where $a_n > 0, z_n > 0$. Since $(z_n - 1) \ln z_n \geq 0$, $\Phi \geq 0$ and vanishes only when $z_n = 1$, which corresponds to the equilibrium point.

2.3. Time-Evolution of the Moments

Next we derive the evolution equations for the first two moments of the length distribution under the assumption that $\kappa_n^+ = \kappa^+$ for all $n < N$ and $\kappa_n^- = \kappa^-$ for all $n \geq 3$. Our approach is similar to that used by Oosawa and Asakura.[18] Let $\mathcal{F}_2$ be the concentration of filaments of length at least two, *i. e.*,

$$\mathcal{F}_2 = \sum_{n=2}^{N} u_n, \tag{8}$$

and let $\mathcal{P}$ be the dimensionless concentration of polymerized actin, which is given by

$$\mathcal{P} = \sum_{n=2}^{N} n u_n = 1 - u_1. \tag{9}$$

The time evolution of $\mathcal{F}_2$ and $\mathcal{P}$ is given by

$$\frac{d\mathcal{F}_2}{d\tau} = \frac{d}{d\tau}\left(\sum_{n=2}^{N} u_n\right) = \sum_{n=2}^{N-1} (j_n - j_{n+1}) + j_N = j_2 = \kappa_1^+ u_1^2 - \kappa_1^- u_2 \tag{10}$$

and

$$\begin{aligned} \frac{d\mathcal{P}}{d\tau} &= \frac{d}{d\tau}\left(\sum_{n=2}^{N} n u_n\right) = -\frac{du_1}{d\tau} = 2j_2 + \sum_{n=3}^{N} j_n \\ &= 2\frac{d\mathcal{F}_2}{d\tau} + (\kappa^+ u_1 - \kappa^-)\mathcal{F}_2 - \underbrace{(\kappa_2^- - \kappa^-)u_3 + \kappa^- u_2 - \kappa^+ u_1 u_N}_{\text{boundary terms}}. \end{aligned} \tag{11}$$

The terms labeled 'boundary terms' represent the contributions from the filament nuclei u_2 and u_3 and the terminal filament u_N that are not included in $\mathcal{F}_2$ and its derivative.

In what follows we assume that

$$\kappa_1^+ = \kappa_1^- = 0 \tag{12}$$

and in effect, turn off the nucleation process. This fixes the number of filaments and facilitates the analysis of the moment evolution. This assumption applies to *in vitro* experimental conditions in which the nucleation pathway is inactivated, and has been used previously in theoretical analysis.[18]

In light of (10) and (12), $\mathcal{F}_2$ is constant and (11) can be rewritten as

$$\frac{d\mathcal{P}}{d\tau} = (\kappa^+ u_1 - \kappa^-)\mathcal{F}_2 - \underbrace{(\kappa_2^- - \kappa^-)u_3 + \kappa^- u_2 - \kappa^+ u_1 u_N}_{\text{boundary terms}} \tag{13}$$

Let X be a non-negative integer-valued random variable defined on the set of filaments that maps every filament of length greater or equal than two to its length, and define the probability measure

$$P(X = n) = \frac{u_n}{\sum_{n=2}^{N} u_n}. \tag{14}$$

Under the assumption given at (12) the expected value of X is given by

$$\mathbb{E}X = \mathcal{P}\mathcal{F}_2^{-1}.$$

Hence, it follows (13) that the evolution of the mean filament length $\mathbb{E}X$ is given by

$$\frac{d\,(\mathbb{E}X)}{d\tau} = (\kappa^+ u_1 - \kappa^-) - \underbrace{(\kappa_2^- - \kappa^-)\frac{u_3}{\mathcal{F}_2} + \kappa^- \frac{u_2}{\mathcal{F}_2} - \kappa^+ \frac{u_1 u_N}{\mathcal{F}_2}}_{\text{boundary terms}}. \tag{15}$$

It is easy to see that

$$\sum_{n=2}^{N} \frac{d(n^2 u_n)}{d\tau} = 2(\kappa^+ u_1 - \kappa^-)\mathcal{P} + 2\kappa^+ u_1 \mathcal{F}_2 - \frac{d\mathcal{P}}{d\tau} - \underbrace{6(\kappa_2^- - \kappa^-)u_3 + 4\kappa^- u_2 - 2(N+1)\kappa^+ u_1 u_N}_{\text{boundary terms}}, \tag{16}$$

and since $\mathcal{F}_2$ is constant, it follows that the second moment

$$\mathbb{E}\left(X^2\right) = \sum_{n=2}^{N} n^2 P(X = n) = \sum_{n=2}^{N} \frac{n^2 u_n}{\mathcal{F}_2} \tag{17}$$

satisfies the evolution equation

$$\frac{d}{d\tau}\left(\mathbb{E}(X^2)\right) = 2(\kappa^+ u_1 - \kappa^-)\frac{\mathcal{P}}{\mathcal{F}_2} + 2\kappa^+ u_1 - \frac{d(\mathbb{E}X)}{d\tau} + \text{boundary terms.} \quad (18)$$

Given the evolution equations for $\mathbb{E}X$ and $\mathbb{E}(X^2)$ one can derive the following equation for the variance $\mathrm{Var}(X)$

$$\frac{d}{d\tau}\mathrm{Var}(X) = \frac{d}{d\tau}\mathbb{E}(X^2) - \frac{d}{d\tau}\mathbb{E}(X)^2. \quad (19)$$

By substituting (15) and (18) into (19) one finds that if (i) the concentration of monomers is critical, and (ii) the boundary terms are negligible, then

$$\frac{d}{d\tau}\mathrm{Var}(X) = \text{ constant} \quad (20)$$

Therefore, under the stated conditions the first two moments of the length distribution evolve according to a diffusion process. As we will see in the next section, this provides an accurate description of the evolution on a long, intermediate time scale, but not early in the evolution from a pure monomer pool, nor in the late stages where boundary effects are important.

3. ANALYSIS OF THE EVOLUTION OF THE LENGTH DISTRIBUTION

3.1. The Early Dynamics

In the remainder of the paper we focus on understanding the different stages in the evolution of the length distribution. Unless stated otherwise, the initial condition for the computational results is a pure monomer pool in a volume of $2000\,\mu\mathrm{m}^3$, which is a typical cell size. We state initial conditions as concentrations, but we present the results in terms of the numbers of a given species. The conversion between these is done by using the fact that 1μM corresponds to 600 molecules/$\mu\mathrm{m}^3$; thus the total number of monomers in the standard volume used is 1.2×10^6.[4] In order to illustrate what is to be understood, we show a computational result for the evolution in Fig. 3. There are three distinct regimes in this figure: the initial stage characterized by formation of the maximum peak height in the distribution, the subsequent polymerization-driven advective phase in which the mean length increases, and a slow final stage in which monomers are redistributed among filaments and the length distribution evolves to the steady-state distribution, which for these initial conditions is a monotone-increasing profile. The objective is to understand the mechanisms underlying these stages, as well

[4] Throughout the numerical computations were done using Gear's method, as implemented in the Livermore solver LSODE.

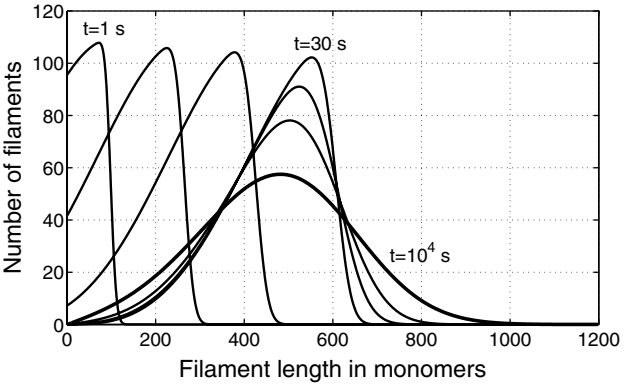

Fig. 3. Time evolution of the filament length distribution. The initial concentration of G-actin is 10 μM. The depicted profiles correspond to 1, 3, 6, 30, 10^3, 3×10^3, and 10^4 secs, respectively. Here and in the following figures $N = 2000$.

as several shorter time-scale early stages and a very long final phase that are not shown in the figure.

The large disparity between the off rates for filaments of length greater than three monomers and those for dimers and trimers leads to four well-defined time scales in the early dynamics, which can be defined in reference to Fig. 4. We lump the species into four pools, comprising monomers, dimers, trimers, and filaments of length four and longer, respectively. The four time scales in increasing order correspond to (i) equilibration of monomers and dimers ($T_1 \sim (k_1^- + 4k^+C_1(0))^{-1} \sim \mathcal{O}(10^{-6})$ sec.), (ii) the time at which the trimers reach their maximum ($T_2 \sim (k_2^- + 9 \cdot k_2^+ K_1 C_1(0)^2)^{-1} \sim \mathcal{O}(10^{-3})$ sec.), (iii) establishment of the total number of filaments (T_3: to be estimated later), and (iv) equilibration of the monomer pool with the filaments (T_4: to be estimated later). T_1 only plays a role in a perturbation analysis done later; for the present we focus on the other scales.

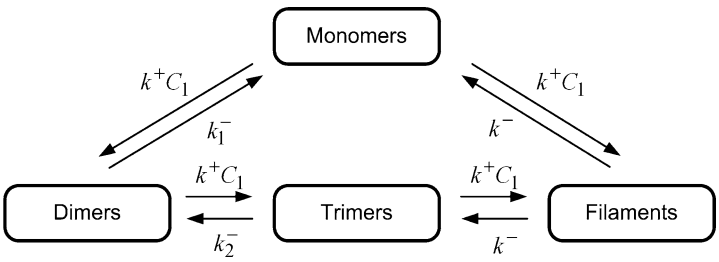

Fig. 4. A schematic of the network for nucleation and filament growth.

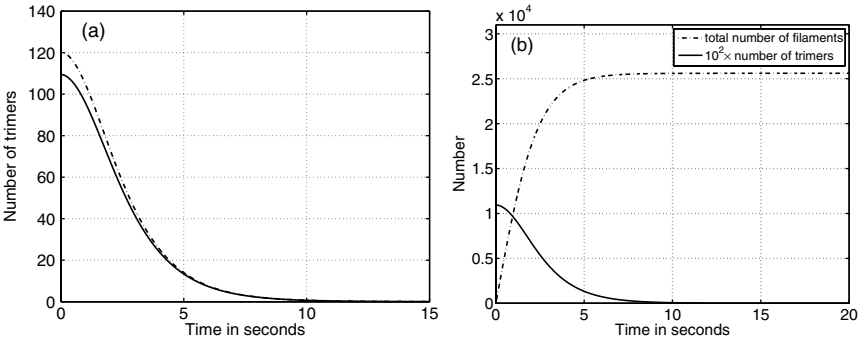

Fig. 5. Time evolution of trimers (a) and the total number of filaments (b) for an initial concentration of G-actin of 10 μM and a volume of 2000 μm^3. In (a) the solid line corresponds to the numerically computed curve, whereas the dashed line corresponds to the approximation given by (21). In both panels the initial rapid rise of trimers is not shown.

On the time scale T_2 the trimer population peaks, and then dimers and trimers equilibrate with the monomer pool, whereas the slower formation of filaments can be neglected on this scale. Thus we can solve the steady-state version of the first three equations in (4) and obtain

$$u_2 = K_1 u_1^2 \qquad u_3 = K_1 K_2 u_1^3. \tag{21}$$

This gives an estimate of the trimers at any time, and in particular, an estimate of the maximum amount of trimers in the system, namely $u_3 = K_1 K_2 u_1^3(0)$. As can be seen in Fig. 5(a) for $C_0 = 10$ μM, (21) provides a very good estimate of the number of trimers except for an initial time interval of order T_2. For an initial concentration of 10 μM, the maximum estimated number of trimers is 120, whereas the computed maximum is approximately 110 (*cf.* Fig. 5(a)). This approximation is acceptable as long as the initial concentration of monomer is not too high, but for an initial concentration of 100 μM the maximum estimated number of trimers is approximately 1.2×10^5, whereas the computed maximum is approximately 5.8×10^4. This is predictable, since by increasing the monomer concentration the trimer-to-filament pathway on Fig. 4 is enhanced and the corresponding dynamics are no longer slow on the time scale characterized by T_2.

In the next phase, during which the trimer concentration tracks that of the monomer as per (21), filaments are formed from the trimers, and the monomer pool decreases due to both filament formation and monomer addition to the growing filaments. The previous estimate of the maximum number of trimers also provides an estimate of the maximum instantaneous rate of filament production, and hence the height of the peak in the filament length distribution. Our numerical computations confirm this approximation: Fig. 3 shows that the peak height

is approximately 110, which agrees with the computed maximum of the trimer population and which is comparable to the theoretical prediction for the maximum number of trimers.

In this phase the trimer concentration or number decreases monotonically and when it reaches a level at which there is only one trimer, the total number of filaments essentially stops increasing. To estimate the end of this phase, which one sees is about 8 secs in Fig. 5(b), we define

$$\mathcal{F}_4 = \sum_{n=4}^{N} u_n \tag{22}$$

and then have

$$\begin{aligned}\frac{du_1}{d\tau} &= -2\left(\kappa_1^+ u_1^2 - \kappa_1^- u_2\right) - \sum_{n=3}^{N}\left(\kappa_{n-1}^+ u_1 u_{n-1} - \kappa_{n-1}^- u_n\right) \\ &= -2j_2 - j_3 - \kappa^+ u_1(u_3 - u_N) - (\kappa^+ u_1 - \kappa^-)\mathcal{F}_4 \qquad (23)\end{aligned}$$

$$\frac{d\mathcal{F}_4}{d\tau} = \kappa_3^+ u_1 u_3 - \kappa_3^- u_4 \tag{24}$$

Since the trimers have already equilibrated with the monomer pool we assume that the fluxes j_2 and j_3 are negligible. We also assume that the non-dimensional concentrations u_3 and u_N are small compared to $\mathcal{F}_4$ and that $u_3 \approx u_4$ at this phase. This leads to the following approximation to the system of (23) and (24).

$$\frac{du_1}{d\tau} = -(\kappa^+ u_1 - \kappa^-)\mathcal{F}_4 \tag{25}$$

$$\frac{d\mathcal{F}_4}{d\tau} = (\kappa^+ u_1 - \kappa^-)K_1 K_2 u_1^3 \tag{26}$$

From (21) one can see that, given the standard parameter values, when the number of trimers is one, $\kappa^- \ll \kappa^+ u_1$. Thus we further approximate the system (25) and (26) as follows.

$$\frac{du_1}{d\tau} = -\kappa^+ u_1 \mathcal{F}_4 \tag{27}$$

$$\frac{d\mathcal{F}_4}{d\tau} = \kappa^+ K_1 K_2 u_1^4 \tag{28}$$

From these one finds that

$$\ln \frac{(1 + (1 - (u_1/u_1(0))^4)^{\frac{1}{2}})}{(1 - (1 - (u_1/u_1(0))^4)^{\frac{1}{2}})} = 4(\kappa^+\kappa^+ K_1 K_2)^{\frac{1}{2}} u_1(0)^2 \tau \tag{29}$$

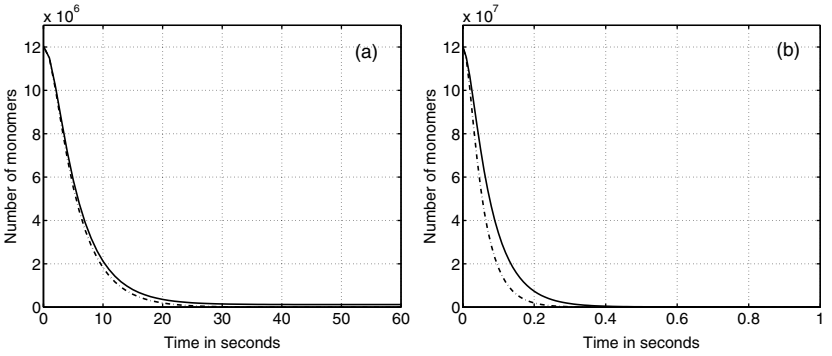

Fig. 6. Time evolution of the G-actin population. The initial concentration of G-actin is set equal to 10 μM on the left and 100 μM on the right. The dashed lines correspond to the theoretical approximation as given by (25) and (26), whereas the solid lines represent the corresponding numerical solutions of the original system.

Using this and (21) shows that the time T_3 needed for the trimer population to drop below one is approximately 6 seconds, which corresponds very well with the computed result shown in Fig. 5(b).

The next phase is characterized by a constant total number of filaments but an increasing mean length of filaments. Now the polymerization reaction pathway in Fig. 4 dominates the dynamics and the maximum in the length distribution propagates outward. During this 'hyperbolic' phase the shape of the length distribution is roughly constant, but the speed of this traveling wave gradually slows as the monomer pool decreases (*cf.* Fig. 7). To understand when this phase ends and the wave stops, note that if there was only one filament, the growth would stop when the monomer concentration reaches the critical level defined earlier. To see that similar considerations apply when many filaments are present, and to predict the time at which the monomer concentration reaches the critical level, we note that the assumptions that led us to approximation (25)–(26), but not the subsequent approximations, are valid in this regime as well.

By integrating Equations (25) and (26) numerically we obtain an estimate of 30 s for the time T_4 needed for the equilibration of the number of monomers. In fact one sees in Fig. 6(a) that this system provides an excellent approximation for u_1 for all but a short initial time interval when the initial concentration of G-actin is 10 μM. For an initial G-actin concentration of 100 μM, the estimated time needed for G-actin equilibration is 0.3 s, but one sees in Fig. 6(b) that the approximation of the time evolution is not as accurate as for an initial concentration of 10 μM. Thus, when the monomer concentration increases ten-fold, the time scale decreases hundred-fold, as can also be seen from the dimensionless on rate κ^+.

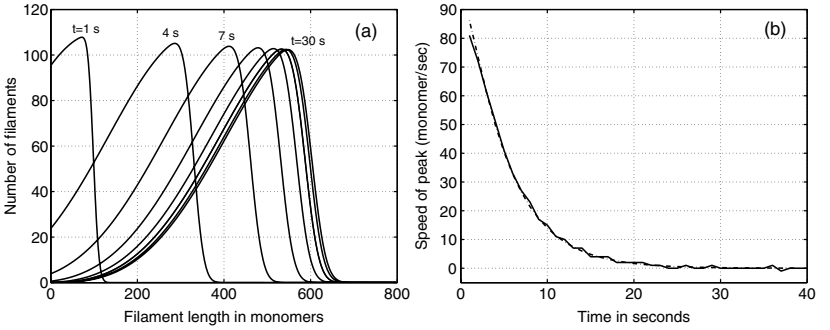

Fig. 7. The convective or hyperbolic phase of the evolution of the length distribution for an initial concentration of 10 μM. The profiles in (a) correspond to 1, 4, 7, 10, 13, 16, 19, and 30 secs, respectively. The speed of the traveling peak is shown in (b), where the solid line corresponds to the speed computed by numerically tracking the peak location, whereas the dashed line corresponds to the theoretical approximation given by the convective term in (30).

To understand the evolution when the filament number is constant, note that for $n \geq 4$ the evolution equations (4) can be written as

$$\frac{du_n}{d\tau} + (\kappa^+ u_1 - \kappa^-)(u_n - u_{n-1}) = \kappa^-(u_{n-1} - 2u_n + u_{n+1}) \tag{30}$$

The second term on the left can be regarded as a convective flux with the time-dependent speed $(\kappa^+ u_1 - \kappa^-)$, whereas the term on the right is diffusion on the graph defined by the kinetic network with diffusion constant κ^-. When $(\kappa^+ u_1 - \kappa^-) > \kappa^-$ convection dominates, but as the monomer concentration approaches the critical level $u_1 = \kappa^-/\kappa^+$, the speed goes to zero and the evolution is dominated by diffusion. Thus one predicts that the hyperbolic phase ends when the monomer reaches the critical level, and ones sees in Fig. 7(a) that this prediction is accurate.

Using the relation between the peak speed and the monomer dynamics, one can approximate the filament length at which the peak stalls by the expression

$$N^* = \int v(t)\mathrm{d}t = \int (k^+ C_1(t) - k^-)\mathrm{d}t \tag{31}$$

If (25) and (26) are used to predict the monomer dynamics, then (31) predicts that $N^* \approx 576$ for $C_0 = 10$ μM, whereas the result obtained from the full system is $N^* \approx 555$. However, for reasons similar to those given earlier, the approximation is not as accurate for $C_0 = 100$ μM, where the predicted value is $N^* \approx 58$ and the actual value is $N^* \approx 68$. Also as before, if C_0 increases ten-fold the time scale decreases hundred-fold, and we expect an approximately ten-fold decrease in N^*.

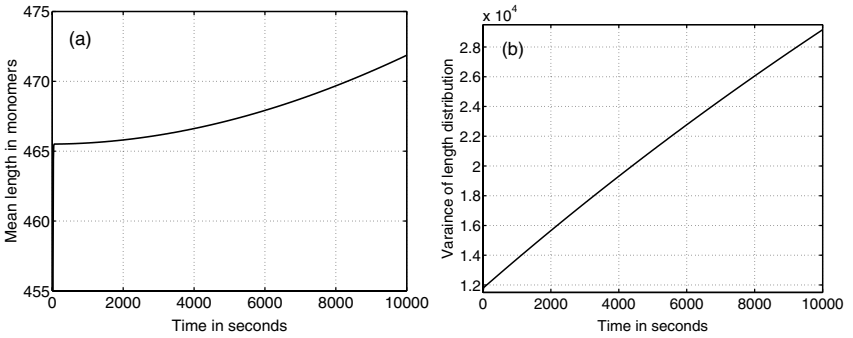

Fig. 8. Time evolution of the mean and variance of the filament length distribution shown in Fig. 3. The evolution of the mean length is shown in (a) and the evolution of the variance is shown in (b).

3.2. The Diffusive Regime

For $C_0 = 10\ \mu$M the hyperbolic phase ends at approximately thirty seconds, and this coincides with the onset of the diffusive reorganization of the length distribution. The dynamics at this stage are characterized by a monomer concentration that is approximately critical, and a fixed number of filaments. The analysis of the moment equations in Sec. 2 indicates that diffusion is the dominant process in this phase, and numerical results for the full system shown in Fig. 8 confirm this. In Fig. 8(a) one sees that the mean length of the distribution only increases about 1% after the first thirty seconds, and the estimated diffusion coefficient is found to be approximately 1 monomer^2/s, as Fig. 8(b) shows.

In the computational experiment that leads to Fig. 8 the initial phases are important, and to completely isolate the diffusion process we have done a numerical experiment in which the initial G-actin concentration is critical and there are 500 filaments of length 800 monomers each. Moreover the nucleation part of the reaction network is switched off, *i. e.*, $\kappa_1^+ = \kappa_1^- = \kappa_2^+ = \kappa_2^- = 0$. According to (30), one predicts that the evolution of the system is governed by a pure diffusion process with mean filament length of 800 monomers and a diffusion constant 1 monomer^2/s. This is seen in Fig. 9, where the diffusion of the initial Dirac function is shown in (a), and the evolution of the variance is shown in (b). This will apply until there are significant boundary effects as described earlier.

To better understand when the diffusive regime applies, we consider the time scale set by the depolymerization rate k^-. It follows from (5) that $\kappa^- = 1$, and we further assume that u_1 has equilibrated at the critical concentration, which implies that system (4)–(5) becomes linear. If we let $u = (u_2, u_3, \cdots, u_N)^T$ and $\Gamma = \left(\kappa_1^+ u_1^2, 0, \cdots 0\right)^T$, then Eq. (4)–(5) are equivalent to

$$\frac{du}{d\tau} = Au + \Gamma \tag{32}$$

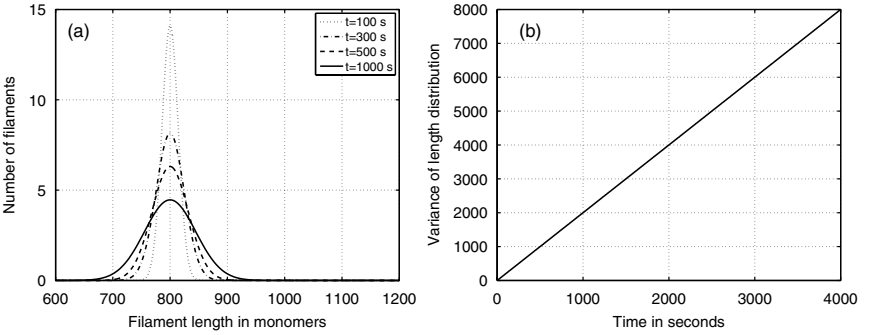

Fig. 9. The evolution of the distribution (a) and the variance (b) beginning with an initial population of 500 filaments of 800 monomers each. As can be seen in (b), the dynamics are clearly diffusive with a linear evolution for the variance, characterized by a slope of 2 monomer^2/s, *i. e.*, a diffusion coefficient of 1 monomer^2/s, as predicted by (30).

where A is the $(N-1)\times(N-1)$ matrix

$$A = \left[\begin{array}{cc|ccccc} -(\kappa^+u_1+\kappa_1^-) & \kappa_2^- & 0 & & & & \\ \kappa^+u_1 & -(\kappa^+u_1+\kappa_2^-) & 1 & 0 & & & \\ \hline 0 & \kappa^+u_1 & -(\kappa^+u_1+1) & 1 & & & \\ & 0 & \kappa^+u_1 & -(\kappa^+u_1+1) & \ddots & & \\ & & & \ddots & \ddots & & \\ & & & & \kappa^+u_1 & -(\kappa^+u_1+1) & 1 \\ & & & & & \kappa^+u_1 & -1 \end{array}\right].$$

We use a perturbation argument to obtain information with respect to the eigenvalues of A. We note that under the specified scaling for time, κ_1^- is of the order of 10^6. We rewrite A in the form

$$A = \epsilon^{-2}(A_0 + \epsilon A_1 + \epsilon^2 A_2)$$

where $\epsilon = \mathcal{O}(10^{-3})$ and

$$A_0 = \left[\begin{array}{cc|ccccc} -1 & 0 & 0 & & & & \\ 0 & 0 & 0 & 0 & & & \\ \hline 0 & 0 & 0 & 0 & & & \\ & 0 & 0 & 0 & & & \\ & & & \ddots & \ddots & & \\ & & & 0 & 0 & 0 & \\ & & & & 0 & 0 & \end{array}\right].$$

Table I. Terms in the perturbation expansion of the eigenvalues

Index	λ_0	λ_1	λ_2
1	-1	0	-1
2	0	-1	-1
$k = 3, N-1$	0	0	α_k

$$A_1 = \left[\begin{array}{cc|ccccc} 0 & 1 & 0 & & & & \\ 0 & -1 & 0 & 0 & & & \\ \hline 0 & 0 & 0 & 0 & & & \\ & 0 & 0 & 0 & & & \\ & & & \ddots & \ddots & & \\ & & & 0 & 0 & 0 & \\ & & & & 0 & 0 & \end{array}\right]$$

$$A_2 = \left[\begin{array}{cc|ccccc} -1 & 0 & 0 & & & & \\ 1 & -1 & 1 & 0 & & & \\ \hline 0 & 1 & -2 & 1 & & & \\ & 0 & 1 & -2 & & & \\ & & & \ddots & \ddots & & \\ & & & 1 & -2 & 1 & \\ & & & & 1 & -1 & \end{array}\right]$$

Let λ_0 be an eigenvalue of A_0 and let x_0 be the associated eigenvector. The eigenvalues are clearly -1 and 0, the latter repeated $N-3$-fold, and both are semisimple. Therefore standard results from perturbation theory[9] show that the eigenvalues and eigenvectors of A can be written in the form

$$\lambda = \lambda_0 + \epsilon\lambda_1 + \epsilon^2\lambda_2 + o(\epsilon^2)$$

$$y = y_0 + \epsilon y_1 + \epsilon^2 y_2 + o(\epsilon^2)$$

An easy calculation shows that the eigenvalues are as given in Table I.
where the α_k are the eigenvalues of the matrix

$$\Delta = \begin{pmatrix} -2 & 1 & & & & \\ 1 & -2 & 1 & & & \\ & 1 & -2 & & & \\ & & & \ddots & & \\ & & & -2 & 1 & \\ & & & 1 & -1 & \end{pmatrix}_{(N-3)\times(N-3)}$$

The eigenvalues and eigenvectors of this matrix can be computed explicitly[19] and are given by

$$\alpha_k = -4\sin^2\left(\frac{\pi(k-5/2)}{2N-5}\right) \qquad k = 3,\ldots,N-1 \tag{33}$$

$$u_{k,l} = \sqrt{\frac{2}{(N-5/2)}}\sin\left(\frac{\pi(k-5/2)l}{N-5/2}\right) \qquad l = 1,\ldots,N-3. \tag{34}$$

Therefore, on the $\mathcal{O}(1)$ time scale there are two large negative eigenvalues corresponding to the relaxation rate of monomer/dimers, and dimers/trimers, respectively, and $N-3$ eigenvalues that arise from the discrete Laplacian Δ. The latter eigenvalues represent the time scales for relaxation of the diffusional modes that characterize the re-shuffling of monomers amongst the filaments during the diffusive phase. Since $\sin x \sim \mathcal{O}(x)$ for $x \ll 1$, the lowest eigenvalues scale as $1/N^2$, and therefore, for $N \sim \mathcal{O}(10^3)$, the lowest modes relax on a time scale of order 10^6 s. This explains the very slow diffusive phase in the evolution of the length distribution, and to further substantiate this, we reconstruct the length distribution at a sequence of times in terms of the eigenfunction of A. As shown on Fig. 10(a) this can be done accurately using only the three slowest modes for $T \sim \mathcal{O}(10^5)$ s ($\sim$ 30 h), but more are required for earlier times. Moreover, Fig. 10(b) shows that this reconstruction is not just a matter of representing the solution at one instant in terms of the eigenfunctions, and thus irrelevant for the dynamics, because it

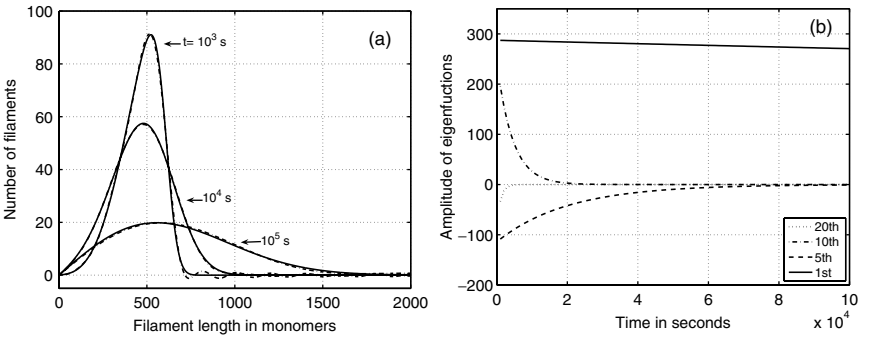

Fig. 10. Reconstruction of the length distribution in terms of the eigenfunctions of the discrete Laplacian at three distinct times (a), and the time evolution of the amplitudes of eigenfunctions needed (b). In (a) the dotted lines represent the reconstruction of the length distribution, whereas the solid lines represent the computational results of length distribution. For t $= 10^3$ s, the filament length distribution is reconstructed using the eigenfunctions corresponding to the lowest 20 eigenvalues given by (34), for t $= 10^4$ s the lowest 10 modes are needed, and for t $= 10^5$ s the three lowest modes suffice. The lowest three eigenvalues are approximately -6.18×10^{-7}, -5.56×10^{-6}, and -1.54×10^{-5}.

shows that the evolution of the amplitudes proceeds as expected in that the higher modes decay rapidly, as predicted by the linear theory.

As a final remark we note that, although the evolution of the mean and variance in Fig. 9 indicates the existence of a diffusion process with a diffusion constant of 1 monomer^2/s, the diffusion-dominated phase in the original experiment, where the nucleation pathway is active, is more complicated than a pure diffusion process. This is due to the existence of the trimer-to-dimer and dimer-to-monomers reaction pathways through which some of the monomers return to the monomer pool. Our numerical computations indicate that the number of filaments in solution decreases by 400 during a time interval of $\sim$10,000 s after the initiation of the diffusion-dominated phase. That is, 400 trimers depolymerize to monomers and, hence, the monomer pool increases by 1, 200 monomers. Of course this number is negligible compared to the $\sim 10^5$ monomers in the monomer pool during the diffusion phase, but, nonetheless, contributes to a small deviation from pure diffusion.

4. OTHER EFFECTS ON THE LENGTH DISTRIBUTION

4.1. The Effect of Imposing a Maximum Length

A question that arises from the preceding analysis is how the imposition of a maximum filament length N less than that which corresponds to having all monomers in one filament affects the various phases in the dynamic. As we found in Sec. 2.1, N determines the monotonicity of the steady-state profile, and specifically, if N is large enough the steady-state length distribution is monotonically decreasing, whereas for N smaller than a critical value the steady-state distribution is monotonically increasing.

The results shown earlier and other computations not reported here show that the early phases in the time evolution, during which the maximum peak height is established and the length distribution propagates to the quasi-attractor state are not affected by the value of N. Moreover, if the maximum N is sufficiently large there will also be a long diffusive redistribution phase before the boundaries affect the evolution. However, since the steady-state profile is affected by N, the diffusion-dominated phase is ultimately affected by the presence of the boundaries as the filament distribution relaxes to the appropriate exponential distribution. This implies that N can affect the time scale associated with the diffusion-dominated phase.

Figure 11 shows the results of a long-time computation of the evolution of the length distribution that illustrates the evolution when the boundaries have a strong influence. In order to establish the exponentially increasing profile, there must be a significant decrease in the total number of filaments to provide the monomers necessary for the long filaments. This in turn requires that there be a significant reverse flux through the trimers and dimers to liberate the required

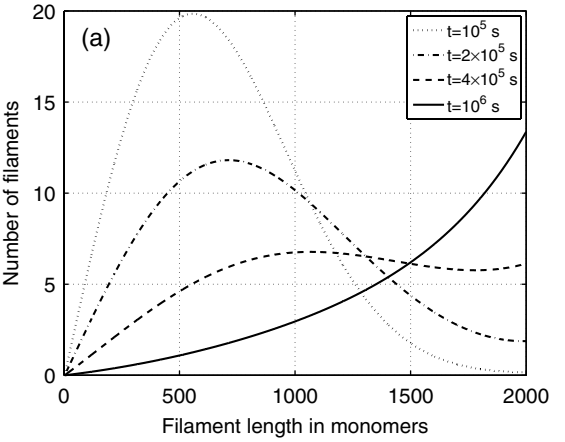

Fig. 11. The long-time dynamics of the filament length distribution for an initial G-actin concentration of 10 μM.

monomers. During this reorganization phase the monomer pool increases above critical again and there is a significant convective flux toward greater filament lengths. In fact, it is apparent from (30) that the monotonically increasing profile reflects a balance between a convective flux to larger N and a diffusive flux down the gradient. During the latter stages of the evolution the mean of the length distribution increases monotonically with time. On the other hand, when the profile is monotone decreasing there is a net convective flux toward the left boundary that is balanced by the diffusive outward flux at the steady state.

4.2. The Effect of Changes in the Nucleation Rate

Nucleation plays a dominant role in the dynamics in that the monomer flux through the filament formation pathway is determined by the net rate of trimer formation. Thus, understanding how altering the rates in this pathway affects the dynamics is important for understanding the effects of accessory proteins such as Arp2/3, which enhance nucleation of free barbed ends. To investigate this in the current framework we decrease the dissociation rates of dimers and trimers so as to stabilize them, and specifically, we set k_1^- equal to 100 s^{-1} and k_2^- equal to 10 s^{-1}.

The results of the computations are shown on Fig. 12, which clearly shows the expected increase in the peak height and a shift of the distribution to shorter lengths. The latter can be understood by noting that the increased rate of filament formation leads to faster depletion of the monomer pool compared with previous computations. Hence, the monomer population reaches the critical level much faster and, according to the analysis in Sec. 2, the mean of the distribution is

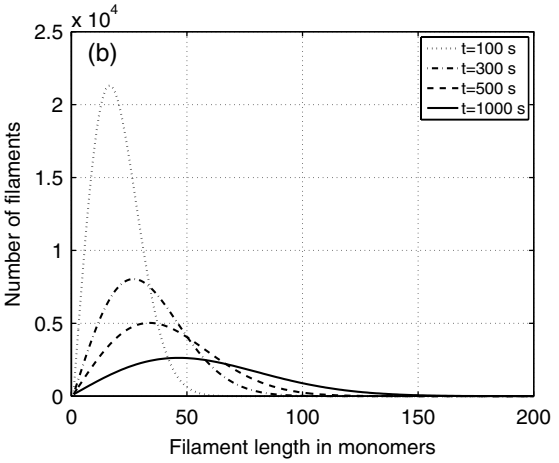

Fig. 12. Dynamics of the filament length distribution with modified nucleation kinetic parameters. Here $k_1^- = 100\ \text{s}^{-1}$ and $k_2^- = 10\ \text{s}^{-1}$ and the initial concentration of G-actin is 10μM.

less than for a lower rate of trimer formation, which produces fewer but longer filaments.

4.3. The Effect of Perturbations in the Monomer Pool

In many eukaryotic cells accessory proteins such as β-thymosins sequester actin monomers to prevent spontaneous nucleation of filaments.[22] Appropriate extracellular or intracellular signals may lead to the release of some of the sequestered actin monomers so as to locally rebuild the actin filament network. In the last computational experiment we illustrate the effect that such a perturbation of the monomer pool has on the filament length distribution.

In this experiment, we consider a solution of 10 μM of actin monomers and let the system evolve for 500 s, during which the intermediate quasi-stationary distribution is established. At 500 s we perturb the monomer pool by adding an additional 10 μM of G-actin to the solution. The dynamics of the length distribution under this protocol are shown in Fig. 13. The perturbation of the monomer pool activates the nucleation pathway and leads to the establishment of a bimodal distribution. Since both the nucleation and the polymerization pathways of the reaction network are active at this stage, the two peaks propagate outward until the monomer pool reaches the critical level. The equilibration of the monomer pool leads, in turn, to the initiation of a diffusion-dominated stage of the evolution during which the two peaks merge into one. The net effect of this transition from the pre-stimulus peak to a new one is an increase of the average filament length.

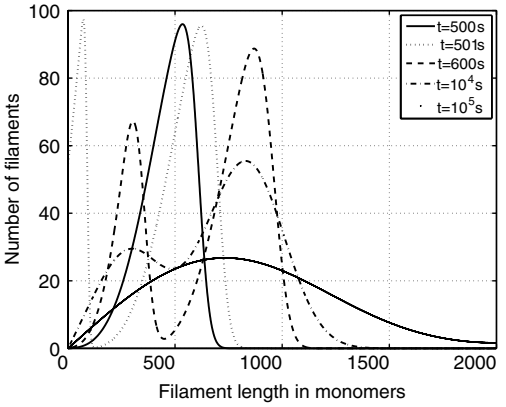

Fig. 13. The effect of perturbing an established profile with a bolus of monomers. Here a system with an initial G-actin concentration of 10 μM evolves for 500 secs, at which time an additional 10 μM of G-actin is injected into the system.

It is clear that such a perturbation may have significant effects on the structure of an existing actin filament network.

5. DISCUSSION

In this paper we analyzed the temporal evolution of the actin filament length distribution in a solution of highly purified monomers. Throughout we used a set kinetic constants for polymerization, depolymerization and nucleation previously reported by Sept *et al.*[24] These constants do not distinguish between barbed and pointed filament ends, and may be interpreted either as the overall rate constants accounting for the dynamics of both barbed and pointed ends, or as kinetic parameters for the dynamics of fast growing barbed ends when pointed ends are assumed to be capped. Both interpretations correspond to experimental configurations investigated previously by others (*cf.*, *e. g.* Ref. 10).

Our primary objective was to understand the relevant time scales for the establishment of the steady-state length distribution. Surprisingly, we found that there are very long-lived intermediate length distributions that are not exponential, even though almost all steady-state distributions are exponentially increasing or decreasing. The analysis shows that there are at least four distinct temporal regimes in the evolution when one begins with a pure monomer pool. In the earliest, which we lump together here, the monomers equilibrate with the dimers and trimers. This is followed by the establishment of the total number of filaments, equilibration of the monomer pool with the filaments, and finally, a long, slow process of equilibration of the length distribution. The second phase is characterized by the

establishment of the early length distribution, and this is followed by a 'hyperbolic' phase in which the total number of filaments changes little, but the distribution 'propagates' with a more-or-less unchanged wave form as the filaments grow. When the monomer pool reaches the critical level the wave stops and the evolution enters the diffusive redistribution phase, during which the amounts in each of the pools in Fig. 4 remains constant, but there is an internal redistribution of monomers amongst filaments of different lengths. We found that this last phase takes 5–6 orders of magnitude longer than the early phases, and we could explain this analytically by doing a spectral analysis of the matrix that results from the $N-3$ equations for the filaments of length ≥ 4. We found that there are eigenvalues of this matrix that are $\mathcal{O}(N^{-2})$, and thus if $N \geq 1000$ or longer the relaxation takes $\mathcal{O}(10^6)$ s. This very slow relaxation implies that experiments done in pure monomer solutions may never reach the equilibrium distribution, and thereby points out the importance of control molecules for rapid establishment of a steady-state *in vivo*.

The analysis was based on the assumption that the system is closed, and therefore the total monomers in all forms is conserved. This implies the existence of an upper bound for the length of actin filaments and the latter was an essential ingredient in our theoretical analysis. As we showed, truncating the distributing numerically is valid in all but the latest stage, where the accessible may determine whether the profile is monotone increasing or decreasing. As we noted earlier, the latter case is important in cases such as filament growth in a vesicle, where there is a relatively small upper bound on the length unless filaments fold during growth. Others have studied the case in which $N \to \infty$, but to our knowledge the detailed temporal evolution of the distribution has not been studied heretofore, either with or without a bound on the admissible filament lengths.

The analysis reported here is the first step toward understanding actin network formation *in vivo*, where nucleation is enhanced by Arp2/3 and there numerous control molecules involved in setting the length distribution and the time scale for establishing the distribution. In work now in progress we are investigating the effects of fragmentation and annealing on the evolution of the length distribution. Estimates of the fragmentation rates show that fragmentation is not important on the time scale for establishment of the quasi-attractor. However, preliminary computational results suggest that whether or not annealing is important depends strongly on the model used for the dependence of the annealing rate on filament length. Using a rate proportional to $1/L$ as in Ref. 24 shows effects of annealing in the early diffusive stages, whereas a rate proportional to $1/L^2$, as in Ref. 8 produces no significant effect of annealing until later in the diffusive stage. This aspect will be investigated further. Another aspect under investigation deals with the dynamics of single filaments, and in particular, the analysis of the effect of nucleotide composition on filament length fluctuations in a stochastic framework. Fujiwara[6] have analyzed experimentally the polymerization dynamics of

individual actin filaments. They report that the time course of polymerization consists of two phases, a relatively rapid polymerization/elongation phase and a subsequent steady-state phase. At the steady-state phase the phenomenon of treadmilling is clearly manifested and, as already mentioned, there exist significant filament length fluctuations of up to the order of 1 μm. In order to explain this dynamic behavior, Fujiwara[6] employ a random-walk description of actin polymerization and focus on the corresponding continuous limit, that is to say, an advection-diffusion partial differential equation. By relating the polymerization kinetic constants at steady state with the diffusion coefficient of the advection-diffusion equation, they conclude that either the effective size of polymerizing units should be larger than that of an actin monomer or that polymerization should proceed through an essentially non-Markovian process, i.e. the dynamics should be dictated by cooperative (consecutive) polymerization and depolymerization events. It has been suggested in the experimental literature that nucleotide profiles convey information for the morphology of actin filament networks and certain reaction pathways, such as filament fragmentation, that apply to the case of individual actin filaments as well.[23]

REFERENCES

1. M. F. Carlier, V. Laurent, J. Santolini, R. Melki, D. Didry, G. X. Xia, Y. Hong, N. H. Chua and D. Pantaloni, Actin depolymerizing factor (ADF/cofilin) enhances the rate of filament turnover: Implication in actin-based motility. *J. Cell Biol.* **136**(6):1307–1322 (1997).
2. H. Chen, B. W. Bernstein, and J. R. Bamburg, Regulating actin-filament dynamics in vivo. *Trends Biochem. Sci.* **25**(1):19–23 (2000). Review.
3. L. P. Cramer, M. Siebert and T. J. Mitchison, Identification of novel graded polarity actin filament bundles in locomoting heart fibroblasts: Implications for the generation of motile force. *J. Cell Biol.* **136**(6):1287–1305 (1997).
4. R. Dickinson, L. Caro and D. Purich, Force generation by cytoskeletal filament end-tracking proteins. *Biophys. J.* **87**:2838–2854 (2004).
5. L. Edelstein-Keshet and G. B. Ermentrout, Models for the length distributions of actin filaments: I. simple polymerization and fragmentation. *Bull. Math. Biol.* **60**(3):449–475 (1998).
6. I. Fujiwara, S. Takahashi, H. Tadakuma, T. Funatsu and S. Ishiwata, Microscopic analysis of polymerization dynamics with individual actin filaments. *Nat. Cell Biol.* **4**(9):666–673 (2002).
7. F. Gerbal, P. Chaikin, Y. Rabin and J. Prost, An elastic analysis of listeria monocytogenes propulsion. *Biophys. J.* **79**(5):2259–2275 (2000).
8. T. L. Hill, Length dependence of rate constants for end-to-end association and dissociation of equilibrium linear aggregates. *Biophys. J.* **44**:285–288 (1983).
9. T. Kato, *Perturbation Theory for Linear Operators*. (Springer-Verlag, Berlin, Germany/Heidelberg, Germany/London, UK etc. 1966).
10. P. Kuhlman, Dynamic changes in the length distribution of actin filaments during polymerization can be modulated by barbed end capping proteins. *Cell Motility Cytoskeleton* **61**:1–8 (2005).
11. L. Limozin, M. Barmann and E. Sackmann, On the organization of self-assembled actin networks in giant vesicles. *Eur. Phys. J. E* (2003).
12. L. M. Machesky and R. H. Insall, Scar1 and the related Wiskott-Aldrich syndrome protein, WASP, regulate the actin cytoskeleton through the Arp2/3 complex. *Curr. Biol.* **8**(25):1347–1356 (1998).

13. A. Mogilner, On the edge: Modeling protrusion. *Curr. Opin. Cell Biol.* **17**:1–8 (2005).
14. A. Mogilner and G. Oster, Cell motility driven by actin polymerization. *Biophys. J.* **71**(6):3030–3045 (1996).
15. A. Mogilner and G. Oster, Force generation by actin polymerization II: The elastic ratchet and tethered filaments. *Biophys. J.* **84**:1591–1605 (2003).
16. K. Moriyama and I. Yahara, Two activities of cofilin, severing and accelerating directional depolymerization of actin filaments, are affected differentially by mutations around the actin-binding helix. *EMBO J.* **18**(23):6752–6761 (1999).
17. R. D. Mullins, J. A. Heuser, and T. A. Pollard, The interaction of Arp2/3 complex with actin: Nucleation, high affinity pointed end capping, and formation of branching networks of filaments. *Proc. Natl. Acad. Sci. USA* **95**(11):6181–6186 (1998).
18. F. Oosawa and S. Asakura, *Thermodynamics of the Polymerization of Protein*. (Academic Press, 1975).
19. H. G. Othmer and L. E. Scriven, Instability and dynamic pattern in cellular networks. *J. Theor. Biol.* **32**:507–537 (1971).
20. A. van Oudenaarden and J. A. Theriot, Cooperative symmetry-breaking by actin polymerization in a model for cell motility. *Nat. Cell Biol.* **1**(8):493–499 (1999).
21. C. S. Peskin, G. M. Odell and G. F. Oster, Cellular motions and thermal fluctuations: The Brownian ratchet. *Biophys. J.* **65**(1):316–324 (1993).
22. T. D. Pollard, L. Blanchoin, and R. D. Mullins, Molecular mechanisms controlling actin filament dynamics in nonmuscle cells. *Annu. Rev. Biophys. Biomol. Struct.* **29**:545–576 (2000). Review.
23. T. D. Pollard and G. G. Borisy, Cellular motility driven by assembly and disassembly of actin filaments. *Cell* **112**(4):453–465 (2003).
24. D. Sept, J. Xu, T. D. Pollard and J. A. McCammon, Annealing accounts for the length of actin filaments formed by spontaneous polymerization. *Biophys. J.* **77**(6):2911–2919 (1999).
25. T. M. Svitkina and G. G. Borisy, Arp2/3 complex and actin depolymerizing factor/cofilin in dendritic organization and treadmilling of actin filament array in lamellipodia. *J. Cell Biol.* **145**(5):1009–1026 (1999).
26. T. M. Svitkina and G. G. Borisy, Progress in protrusion: The tell-tale scar. *Trends Biochem. Sci.* **24**(11):432–436 (1999). Review.
27. M. D. Welch, A. Mallavarapu, J. Rosenblatt and T. J. Mitchison, Actin dynamics in vivo. *Curr. Opin. Cell Biol.* **9**(1):54–61 (1997).
28. E. G. Yarmola and M. R. Bubb, Profilin: Emerging concepts and lingering misconceptions. *Trends Biochem. Sci.* **31**(4):198–205 (2006).